analytical chemistry

pubs.acs.org/ac Article

Flow Field-Flow Fractionation with a Thickness-Tapered Channel

Seung Yeon Shin, Jae Won Seo, Jin Yong Kim, Philip Stephen Williams, and Myeong Hee Moon*

Cite This: *Anal. Chem.* 2022, 94, 14460−14466 Read Online

ACCESS | Metrics & More | Article Recommendations

ABSTRACT: This study introduces the thickness-tapered channel design for flow field-flow fractionation (FlFFF) for the first time. In this design, the channel thickness linearly decreases along the channel axis such that the flow velocity increases down the channel. Channel thickness is an important variable for controlling retention time and resolution in field-flow fractionation. Especially, in the steric/hyperlayer mode of FlFFF, in which particles (>1 μm) migrate at elevated heights above the channel wall owing to hydrodynamic lift forces, the migration of long-retaining smaller-sized particles can be enhanced in a relatively thin channel or by increasing the migration flow rate; however, an upper size limit that can be resolved is simultaneously sacrificed. A thickness-tapered channel was constructed without a channel spacer by carving the surface of a channel block such that the channel inlet was deeper than the outlet (w = 400 → 200 μm). The performance of a thickness-tapered channel was evaluated using polystyrene standards and compared to that of a channel of uniform thickness (w = 300 μm) with a similar effective channel volume in terms of sample recovery, dynamic size range of separation, and steric transition under different flow rate conditions. The thickness-tapered channel can be an alternative to maintain the resolving power for particles with an upper large-diameter limit, faster separation of particles with a lower limit, and higher elution recovery without implementing the additional field-programming option.

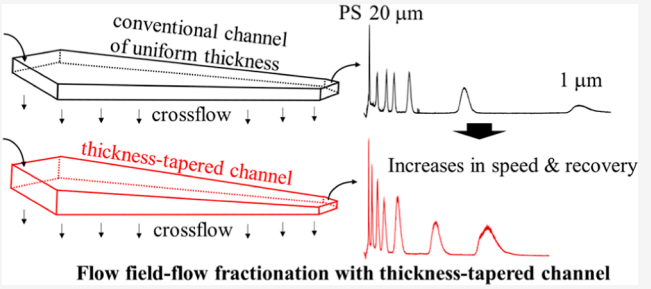

Flow field-flow fractionation with thickness-tapered channel

Flow field-flow fractionation (FlFFF) is an elution-based method that can separate macromolecules by size.[1−3] It is the most popularly used variant of field-flow fractionation (FFF) techniques because of its wide variety of applications including synthetic polymers, proteins, subcellular and extracellular vesicles, cells, and nano- to micron-sized particles.[4−8] Size-based separation in FlFFF is based on the differential distribution of sample components above the channel wall depending on their hydrodynamic diameters, as well as enforcement by crossflow moving across the channel wall. When migration flow of a parabolic velocity pattern is applied to sample components that are in equilibrium between the force (crossflow) and opposing diffusional forces, submicron-sized particles or macromolecules elute with an increasing order of diameter, which is typical during elution in the normal operating mode of FFF.[1] However, particles larger than ∼1 μm in diameter elute in an opposite order of sizes owing to the negligible contribution of particle diffusion but increased role of hydrodynamic lift forces,[9] called steric/hyperlayer operation.[10]

As mentioned, diffusion does not play a significant role in the mechanism of elution of particles larger than ∼1 μm in diameter. Such particles are driven to equilibrium positions close to the accumulation wall where the force due to the applied field or the drag due to the fluid crossflow is balanced by opposing hydrodynamic lift forces. While fluid inertial lift forces tend to drive particles away from walls bounding fluid flow, they are relatively weak and are often not strong enough to counter the applied forces.[9] Experiments using sedimentation FFF have shown the effect of much stronger lift forces in the region close to the wall. These forces appear to increase with particle volume, to increase with the reciprocal of the distance between an entrained particle and the wall, and to increase with the fluid shear rate close to the wall.[11] The result is that the equilibrium positions of the particles are generally quite close to the wall. The consideration of hydrodynamic effects that retard the particle velocity relative to that of the undisturbed fluid velocity at the position of the particle center then determines its migration velocity along the channel.[11,12] The observation that diameter-based selectivity S_d (= $d \log t_r/d \log d$) tends to be less than unity in steric sedimentation FFF and greater than unity in steric/hyperlayer flow FFF is consistent with this model.[13,14]

When analyzing particulate or cellular species with a diameter range of ∼1 μm, complete separation either by the normal or steric/hyperlayer mode alone is difficult because of

Received: August 11, 2022
Accepted: September 22, 2022
Published: October 4, 2022

https://doi.org/10.1021/acs.analchem.2c03503
Anal. Chem. 2022, 94, 14460−14466

the coelution of particles around the steric inversion diameter. The steric inversion diameter in FlFFF was typically observed in 0.4−0.7 μm of polystyrene (PS) latex beads.[15−17] The steric inversion diameter can be increased by decreasing the hydrodynamic lift forces either by increasing the channel thickness or by increasing diffusional contribution by increasing temperature; this diameter increased up to 1.8 μm when the channel thickness was increased to 490 μm.[18] This approach can be useful for the size analysis of submicron-sized sample materials with some oversized species of approximately 1−2 μm in diameter. However, for particle samples with primary size distributions exceeding 1 μm, including those with some undersized (<1 μm) particles as a minor distribution, it is useful to shift steric inversion to a low submicrometer scale. Such operation can be achieved via increasing hydrodynamic lift forces[9] by decreasing the channel thickness or increasing the migration flow velocity. Steric inversion was reduced to ∼0.23 μm for PS latex by decreasing channel thickness in FlFFF.[15] However, when the channel thickness is decreased, the upper particle size that can be resolved is limited. Increasing the field strength can be an alternative to overcome this limitation, but this approach may increase the risk of sample loss in the channel if the migration flow velocity is not high, despite the simultaneous increase in the hydrodynamic lift forces for larger-diameter particles. An alternative approach to enlarge the dynamic size range of separation without sacrificing the retention time for smaller particles and resolution for larger particles in the steric/hyperlayer mode is by employing a field-programming method in which either the crossflow rate decreases or the migration flow rate increases with time.[4,19,20] However, flow rate programming for FlFFF requires a special flow controller that incurs an additional cost for the system setup.

This study introduced the development of a thickness-tapered FlFFF channel for the first time. In this designed channel, the channel thickness linearly decreases along the channel axis; thus, the linear flow velocity increases. This effect enhances the migration of long-retaining species without employing a programmed increase in migration flow or a programmed decrease in field strength. Because a gradual increase in the migration flow rate during separation lowers the detector signals owing to a dilution effect, a thickness-tapered FlFFF channel can be an alternative approach for enhancing particle separation without increasing the outflow rate or decreasing the field strength. The thickness-tapered FlFFF channel was constructed by carving the channel space below the surface of the upper channel block of an asymmetrical FlFFF channel such that the depth (w = 400 μm) of the channel inlet was higher than that (w = 200 μm) of the outlet. Therefore, the typical channel spacer used for constructing the channel space was removed in the thickness-tapered FlFFF channel. The performance of a thickness-tapered FlFFF channel (w = 400 → 200 μm) was compared with that of a conventional FlFFF channel possessing uniform thickness (w = 300 μm) and a similar void volume by examining the dynamic size range of particle separation under different flow rate conditions, steric transition diameters, and particle recoveries using a set of PS latex standards with a broad diameter range (0.020−20 μm in diameter).

THEORY

Typical channel geometries of FlFFF are rectangular (fixed breadth) or trapezoidal (decreasing breadth) designs with a fixed channel thickness. Between the two, the trapezoidal geometry is more commonly utilized. A thickness-tapered FlFFF channel with a trapezoidal breadth can be constructed without using a typical channel spacer by carving the channel space inside the channel block, as shown in Figure 1a, and the

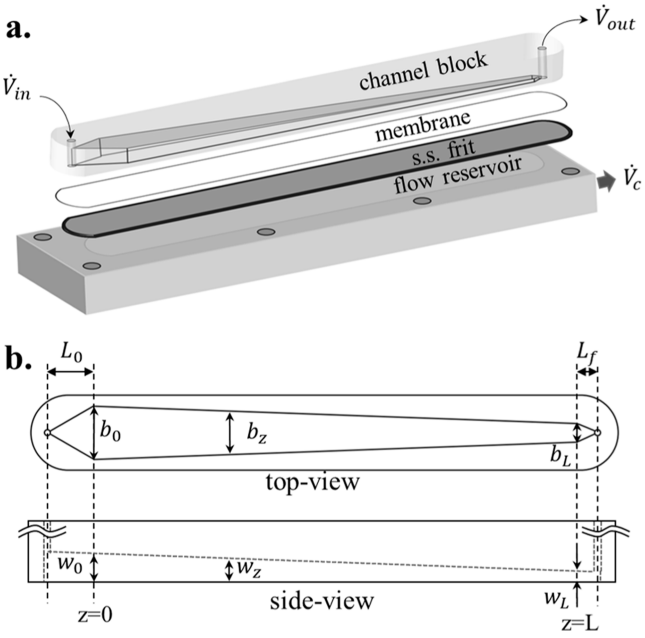

Figure 1. (a) Schematics of a thickness-tapered FlFFF channel, in which a channel space is carved by decreasing thickness, and (b) the top and side views of a channel block.

dimensions of the channel geometry are shown in Figure 1b. As indicated by the channel dimensions in Figure 1b, b_0 and b_L are the channel breadths at z = 0 and z = L, respectively. L_0 and L_f, which are the lengths of end pieces at the inlet and outlet, respectively, were adjusted to be the same as b_0 and b_L, and this adjustment was applied for both rectangular and trapezoidal channels. Similarly, w_0 and w_L are the thicknesses at z = 0 and L, respectively. Here, L is the effective channel length, which is defined as the distance between the start (z = 0) of the separation without including the inlet end piece and the last (z = L) of separation without considering the outlet end piece, according to Williams.[21] In this configuration, the volumetric channel flow rates at z = 0 and z = L are expressed as $\dot{V}_0$ and $\dot{V}_L$, respectively. $\dot{V}_0$ can be calculated from $\dot{V}_{in}$, the flow rate at the channel inlet by subtracting the portion of the crossflow rate exiting through the inlet end piece.

For the following derivation, we assume that the sample focusing/relaxation occurs at z = 0, as defined by Figure 1b, and that the particles migrate along the channel to z = L under elution flow conditions.

Because the channel breadth and thickness decrease along the channel length as a function of position z, the local mean flow velocity, $\langle v \rangle_z$, is expressed as follows:

$$\langle v \rangle_z = \frac{\dot{V}_z}{b_z w_z} \tag{1}$$

where $\dot{V}_z$ is the volumetric flow rate at any arbitrary position z and $b_z w_z$ represents the cross-sectional area at z. When the channel breadth linearly decreases from b_0 to b_L, the channel breadth can be expressed as

https://doi.org/10.1021/acs.analchem.2c03503
Anal. Chem. 2022, 94, 14460−14466

$$b_z = b_0 - (b_0 - b_L)\frac{z}{L} \tag{2}$$

Similarly, the thickness of a channel with decreasing thickness from w_0 to w_L can be expressed as

$$w_z = w_0 - (w_0 - w_L)\frac{z}{L} \tag{3}$$

In eq 1, the volumetric flow rate at any arbitrary position z, $\dot{V}_z$, is expressed as follows:

$$\dot{V}_z = \dot{V}_0 - \frac{A_z}{A_e}(\dot{V}_0 - \dot{V}_L) \tag{4}$$

where A_z is the channel area from $z = 0$ up to any point z, A_e is the effective channel area between $z = 0$ and $z = L$, and $\dot{V}_0 - \dot{V}_L$ is the volumetric flow rate lost by the effective channel area from z = 0 to $z = L$. A_z is now expressed as

$$A_z = \frac{(b_0 + b_z)}{2}z \tag{5}$$

and A_e is simply expressed as

$$A_e = \frac{(b_0 + b_L)}{2}L \tag{6}$$

Similarly, the effective channel void volume V^0 is defined as the volume above the effective channel area and can be simply obtained by

$$V^0 = \int_0^L b_z w_z \, dz = \frac{L}{6}\{b_0(2w_0 + w_L) + b_L(w_0 + 2w_L)\} \tag{7}$$

The local mean flow velocity, $\langle v\rangle_z$, in eq 1 can be calculated using eqs 2 to 6 as follows:

$$\langle v\rangle_z = \frac{(b_0 + b_L)\dot{V}_0 - \left\{2b_0\frac{z}{L} - (b_0 - b_L)\frac{z^2}{L^2}\right\}(\dot{V}_0 - \dot{V}_L)}{\left\{b_0 - (b_0 - b_L)\frac{z}{L}\right\}\left\{w_0 - (w_0 - w_L)\frac{z}{L}\right\}(b_0 + b_L)} \tag{8}$$

Equation 8 not only applies to a thickness-tapered channel but also to any channel design with constant thickness.

Because the channel flow velocity with decreasing thickness continuously changes along the migration axis, the normalized flow velocity profile can be useful for estimating the change in the flow velocity profile along the channel axis. The normalized flow velocity profile can be obtained from the ratio of the local flow velocity $\langle v\rangle_z$ given by eq 8 to the time-averaged velocity $\langle\overline{v}\rangle$ $(=L/t^0)$ as[21]

$$\frac{\langle v\rangle_z}{\langle\overline{v}\rangle} = \frac{\langle v\rangle_z}{L/t^0} \tag{9}$$

The void time of a typical asymmetrical channel (either trapezoidal or rectangular) with uniform thickness is calculated as[22]

$$t^0 = \frac{V^0}{\dot{V}_0 - \dot{V}_L}\ln\left(\frac{\dot{V}_0}{\dot{V}_L}\right) \text{ (uniform thickness)} \tag{10}$$

Equation 10 is not valid for a channel with decreasing thickness; therefore, the t^0 of a channel with decreasing thickness is expressed as

$$t^0 = \int_0^L \frac{dz}{\langle v\rangle_z} = \int_0^L \frac{b_z w_z \, dz}{\dot{V}_z} \text{ (thickness-tapered)} \tag{11}$$

Equation 11 can be solved by numerical analysis. Therefore, eq 9 is now expressed as

$$\frac{\langle v\rangle_z}{\langle\overline{v}\rangle} = \frac{\langle v\rangle_z}{L/t^0} = \frac{t^0}{L} = \frac{(b_0 + b_L)\dot{V}_0 - \left\{2b_0\frac{z}{L} - (b_0 - b_L)\frac{z^2}{L^2}\right\}(\dot{V}_0 - \dot{V}_L)}{\left\{b_0 - (b_0 - b_L)\frac{z}{L}\right\}\left\{w_0 - (w_0 - w_L)\frac{z}{L}\right\}(b_0 + b_L)} \tag{12}$$

Although a complete solution of 12 cannot be derived, the normalized velocity profile of a trapezoidal channel with tapering thickness can only be plotted against z/L by incorporating numerical analysis. When 12 is solved for the case of uniform thickness $(w_0 = w_L)$, the equation is derived as

$$\frac{\langle v\rangle_z}{\langle\overline{v}\rangle} = \ln\left(\frac{\dot{V}_0}{\dot{V}_L}\right)\left\{\frac{1 + (b_L/b_0)}{2(1 - (\dot{V}_L/\dot{V}_0))} - \frac{z}{L} + \frac{1 - (b_L/b_0)}{2}\frac{z^2}{L^2}\right\}\times\left[\left\{1 - \left(1 - \frac{b_L}{b_0}\right)\frac{z}{L}\right\}\right]^{-1} \tag{13}$$

which is identical to the expression found in ref21.

EXPERIMENTAL SECTION

Materials and Reagents. An AF4 channel (model LC) from Wyatt Technology Europe GmbH (Dernbach, Germany) was modified by replacing the accumulation wall inlay with a homemade polycarbonate block engraved with the shape of a typical ribbon-like channel space without using a spacer. All channel spaces were carved from the surface of the channel block in a trapezoidal shape with an initial and final breadths (b_0 and b_L, respectively) of 2.1 and 0.6 cm, respectively, in a tip-to-tip channel length of 26.6 cm. The lengths of the triangular end pieces of a channel for the inlet and outlet triangles were L_0 = 2.1 cm and L_f = 0.6 cm, respectively. A thickness-tapered channel was constructed, where the inlet was the deepest and the outlet was the shallowest, indicating decreasing channel thickness. The thicknesses of the tapered channels at the inlet (w_{in}) and outlet (w_{out}) were w_{in}/w_{out} = 400/200 μm. A channel of uniform thickness (300 μm) was constructed in the same manner as the thickness-tapered channel without using a spacer. The total geometrical void volumes, including end pieces, were 1.09 and 1.04 cm^3 for the thickness-tapered and uniform channels, respectively. The channel membrane was a regenerated cellulose membrane (MWCO, 10 kDa), purchased from Wyatt Technology Europe GmbH. After each FlFFF run, the membrane was rinsed for 10 min without crossflow. The thickness-tapered channel was evaluated using PS standard beads with nominal diameters of 0.023, 0.051, 0.100, 0.203, 0.303, 0.400, 0.508, 0.600, 0.799, 0.994, 1.999, 4.000, 6.007, 7.979, 10.15, 12.01, and 20.00 μm (hereafter referred to as 20, 50, 100, 200, 300, 400, 500, 600, and 800 nm, and 1, 2, 4, 6, 8, 10, 12, and 20 μm) purchased from Thermo Fisher Scientific (Waltham, MA, USA). The carrier solution was 0.05% sodium dodecyl sulfate (SDS) and

https://doi.org/10.1021/acs.analchem.2c03503
Anal. Chem. 2022, 94, 14460−14466

0.02% sodium azide (NaN_3) purchased from Sigma-Aldrich (St. Louis, MO, USA) and prepared using ultrapure water (>18 MΩ·cm). The solution was filtered using a 0.22 μm pore size mixed cellulose ester (MCE) membrane filter from MF-Millipore (Danvers, MA, USA) via a 2522C-10 vacuum pump (Welch, Louisiana, USA) and degassed for 1 h using a degasser from Branson (Danbury, CT, USA) prior to FlFFF runs. Sample injection was performed using a model 7725i injector (Rheodyne, Cotati, CA, USA) with a sample loop (25 μL). PS standards were injected during the focusing/relaxation mode, in which the carrier solution was delivered to both the channel inlet and outlet at a 1:9 ratio of the flow rate required for the separation such that the injected particles were focused at the 1/10 position from the channel inlet. The carrier solution was delivered using a model SP930D HPLC pump. The PS particles were detected using a model YL9120 UV−Vis detector at 254 nm and recorded using Autochro-3000 software (Young-Lin Instruments, Seoul, Korea).

The focusing flow rate ratio allows the calculation of the focusing position in the channels. The channel length and breadth dimensions correspond to a total channel area of 34.65 cm^2. The focusing position must therefore correspond to an area, measured from the inlet, of 3.465 cm^2. This places the focusing position at 2.71 cm from the inlet, or 0.61 cm beyond the inlet end piece, within the trapezoidal section of the channels. When z is defined as zero at the focusing position, L is defined as the distance from the focusing position to the start of the outlet end piece, and b_0, w_0, and $\dot{V}_0$ correspond to $z = 0$, then all eqs 1 to 13 remain valid and refer to the effective region of elution along the channels, ignoring the small outlet end pieces. Therefore, $L = 23.29$ cm, $b_0 = 2.06$ cm, $w_0 = 0.0380$ cm, and $w_L = 0.0205$ cm for the thickness-tapered channel, and $\dot{V}_0$ is given by either $\dot{V}_{in} - 0.1\dot{V}_c$, where $\dot{V}_{in}$ is the channel inlet flow rate during elution, or $\dot{V}_{out} + 0.9\dot{V}_c$, where $\dot{V}_{out}$ is the channel outlet flow rate during elution. Note that with this redefinition of z, the effective channel volumes given by eq 7 are then found to be 0.955 and 0.930 cm^3 for the thickness-tapered and uniform channels, respectively.

RESULTS AND DISCUSSION

The performance of a thickness-tapered FlFFF channel was evaluated with PS latex standards in comparison to a conventional channel with uniform thickness. Figure 2a shows the fractograms of PS separation in the steric/hyperlayer mode of FlFFF obtained with a uniform channel ($w = 300$ μm, top) and a thickness-tapered channel ($w = 400 \rightarrow 200$ μm, bottom) at an outflow rate ($\dot{V}_{out}$)/crossflow rate ($\dot{V}_c$) of 3.0/0.5 mL/min. Compared with the separation in the uniform channel, the retention of PS particles in the thickness-tapered channel was reduced by approximately 29% on average with an increase in peak intensities for most particles. This was in spite of a 2% higher calculated effective void time of 0.294 min using eq 11 for the tapered channel compared with 0.288 min for the uniform channel. In particular, the retention time of PS 1.0 μm was considerably reduced by 40%, indicating that the hydrodynamic lift forces for long-retaining species were effective in the thickness-tapered channel under identical flow rate conditions. The decrease in retention time in the thickness-tapered channel was approximately 36% on average when the outflow rate was increased to 4.5 mL/min (Figure 2b). This 36% decrease in retention time occurred when the calculated effective void time increased again by 2% from 0.197 min for the uniform channel to 0.201 min for the tapered channel.

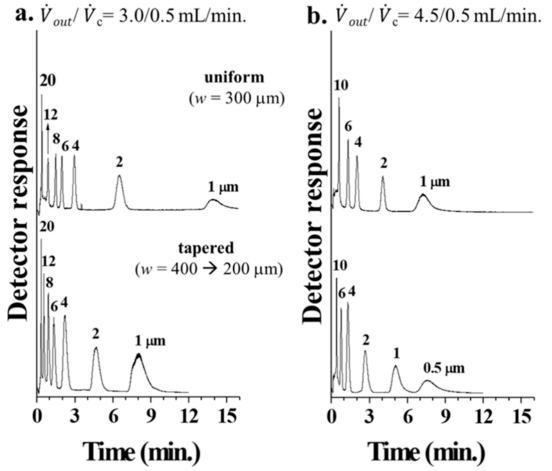

Figure 2. Comparison of steric/hyperlayer separation of PS standard mixtures obtained between the uniform ($w = 300$ μm) and thickness-tapered ($w = 400 \rightarrow 200$ μm) channels at two different flow rate conditions: (a) $\dot{V}_{out}/\dot{V}_c = 3.0/0.5$ mL/min and (b) $\dot{V}_{out}/\dot{V}_c = 4.5/0.5$ mL/min.

With further increase in the lift forces from the increase in the migration flow velocity, PS 0.5 μm particles were successfully resolved in the thickness-tapered channel. Figure 2 shows that the separation of long-retaining components (<2 μm) can be successfully achieved in the thickness-tapered channel without further increasing the migration flow rate or decreasing the crossflow rate. Both approaches may deteriorate the resolution of early eluting components, which may reduce the upper size limit of separation. Moreover, an increase in migration flow rate results in a dilution effect in typical UV detectors. Because the thickness-tapered channel was thicker at the inlet and thinner at the outlet by 100 μm each compared with those of the uniform thickness channel ($w = 300$ μm), particle migration in the thickness-tapered channel was more sluggish before half of the channel length but faster in the second half of the channel than that in the uniform thickness channel. Moreover, during the relaxation and initial migration of particles in the first half of the thickness-tapered channel, it is expected to provide a better differentiation of equilibrium heights for particles of different sizes against the accumulation wall than in the uniform thickness channel. This effect can maintain the separation resolution of early eluting particles (for instance PS 10 μm in Figure 2b). Therefore, by implementing a thickness-tapered channel, the dynamic size range of separation can be expanded to smaller sizes in the steric/hyperlayer separation of FlFFF, and the effect of programming the channel flow rate can be achieved without incurring the dilution effect during detection.

Variations in the local mean flow velocity along the axis of migration in the uniform and thickness-tapered channels can be compared by plotting the normalized velocity profile $\frac{\langle v \rangle_z}{\langle \bar{v} \rangle}$, using eqs 12 and 13 with computer simulation as a function of fractional length z/L, in Figure 3. The solid line in Figure 3 is the normalized velocity profile of the thickness-tapered channel ($w = 400 \rightarrow 200$ μm) under the run conditions utilized in Figure 2a, whereas the dashed line represents the uniform thickness channels ($w = 300$ μm). The breadths of both channels were trapezoidal ($b_L/b_0 = 0.29$). For

https://doi.org/10.1021/acs.analchem.2c03503
Anal. Chem. 2022, 94, 14460−14466

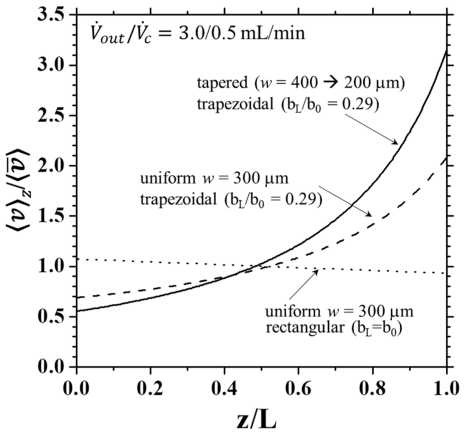

Figure 3. Plots of the normalized mean channel flow velocity $\langle v \rangle_z / \langle \overline{v} \rangle$ as a function of z/L for trapezoidal channels with uniform thickness (300 μm) and tapering thickness (400 → 200 μm, w_L/w_0 = 0.54) with a fixed b_L/b_0 = 0.29 compared with the plot for a rectangular channel with uniform thickness. The flow rate condition for all cases is fixed at $\dot{V}_{out}/\dot{V}_c$ = 3.0/0.5 mL/min.

comparison, the velocity profile of a rectangular ($b_L = b_0$) channel with uniform thickness was plotted together using the dotted line in Figure 3. The normalized flow velocity of a rectangular channel with uniform thickness sluggishly decreased at $\dot{V}_{out}/\dot{V}_c$ = 3.0/0.5 in mL/min, in which the loss of migration flow velocity along the channel axis by the exit of crossflow was not significantly large owing to the use of a relatively higher outflow rate compared to the crossflow rate. For the uniform thickness channel with a trapezoidal breadth, the initial migration velocity was lower than the average migration velocity before the middle point of channel; however, migration velocity rapidly increased in the last half of the channel length compared to that of the rectangular channel. The normalized flow velocity of the thickness-tapered channel was not significantly lower in the first half of the channel length than that of the uniform thickness, even though the inlet thickness of the thickness-tapered channel was greater than that of the uniform thickness channel by 100 μm. However, its increase was more rapid than that in the remainder of the channel. Because of the similarity in effective void volumes of the two channels (0.930 and 0.955 cm^3 for the uniform and thickness-tapered channels, respectively), the difference in the time-averaged velocity, $\langle \overline{v} \rangle$, between the two channels was not significant. (Effective void times differ by just 2% as mentioned earlier.) Therefore, the normalized flow velocity profiles for the two trapezoidal channels (uniform and thickness-tapered) represent the variations in local mean flow velocity, $\langle v \rangle_z$. Based on these findings, the mean flow velocity at the beginning of the thickness-tapered channel can be inferred not to be significantly lower than that in the uniform channel despite the difference in channel thicknesses, rapidly increasing in the second half of the channel; this increase in flow velocity was conducive to the recovery of long-retaining particles due to the increased contribution of lift forces. The recovery of particle elution was determined by calculating the relative ratio of the peak area of each PS standard particle obtained at a given crossflow rate to that of the same standard obtained without applying crossflow at a fixed outflow rate for the datasets shown in Figure 2. Figure 4 shows that elution recovery generally decreases with decreasing particle size or with increasing retention in the steric/hyperlayer mode. The

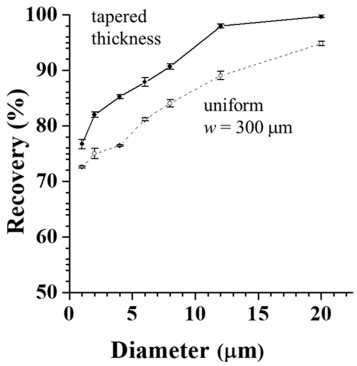

Figure 4. Recovery values (%) of PS standards calculated from the peak area of each species between the uniform (w = 300 μm) and thickness-tapered (w = 400 → 200 μm) channels obtained at $\dot{V}_{out}/\dot{V}_c$ = 3.0/0.5 mL/min.

recovery values of the PS standards in the thickness-tapered channel appeared to exceed 80%, except for that of PS 1 μm, of those obtained in the uniform channel, and the average recovery value for the steric/hyperlayer run was higher by ~8% in the thickness-tapered channel.

The thickness-tapered channel was tested using submicron PS standard mixtures under two different operating conditions (Figure 5). With the uniform thickness channel, PS particles

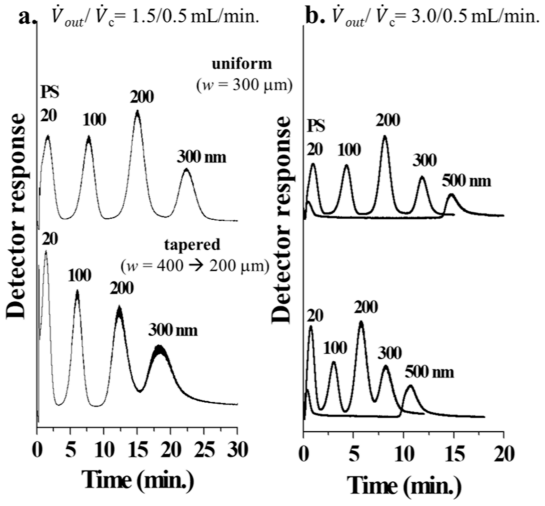

Figure 5. Normal mode separation of submicron-sized PS standard mixtures compared between the uniform (w = 300 μm) and thickness-tapered (w = 400 → 200 μm) channels under the two different flow rate conditions: (a) $\dot{V}_{out}/\dot{V}_c$ = 1.5/0.5 mL/min and (b) $\dot{V}_{out}/\dot{V}_c$ = 3.0/0.5 mL/min.

with diameters ranging from 20 to 300 nm were well separated at a baseline resolution of $\dot{V}_{out}/\dot{V}_c$ = 1.5/0.5 mL/min; however, the separation of the same mixtures using the thickness-tapered channel was achieved with relatively poor resolution, especially for PS 200 and 300 nm particles. This poor resolution is attributed to the increased contribution of hydrodynamic lift forces owing to the decrease in channel thickness toward the channel outlet. An increase in the outflow rate to 3.0 mL/min (Figure 5b) resulted in the high-speed separation of PS mixtures at a similar resolution to that shown in Figure 5a for the uniform thickness channel. Due to the increase in steric effect, PS 500 nm particles were eluted much earlier than was

https://doi.org/10.1021/acs.analchem.2c03503
Anal. Chem. 2022, 94, 14460−14466

expected from the theory where the retention time in FlFFF linearly increases with diameter.[23] An improvement of the particle migration in the normal mode can be achieved by decreasing the outflow rate which would have the effect of reducing the lift forces on particles larger than 300 nm in particular.

Figure 5 shows that the performance of the thickness-tapered channel in the normal mode of separation is relatively poor compared to that of the uniform channel. Given that the flow velocity after the middle point of a thickness-tapered channel increases much faster than that of a uniform channel with a similar void volume (Figure 3), the influence of the hydrodynamic lift forces can be larger in the thickness-tapered channel. To examine steric inversion in the thickness-tapered channel, retention times of 16 PS standards ranging from 0.020 to 20 μm obtained under the run conditions used in Figure 2a were plotted against diameter in logarithmic scale in Figure 6.

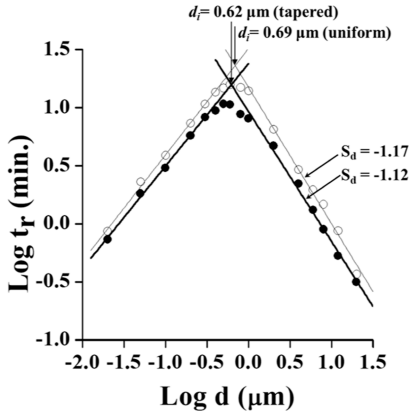

Figure 6. Plot of log t_r (min) vs log d (μm) of PS standards (0.02−20 μm in diameter) obtained between the uniform and thickness-tapered channels marked with the empirical steric inversion diameter (d_i) values. The run conditions are the same as those used in Figure 2a.

Diameter selectivity, as indicated by the slope S_d (= d log t_r/d log d) of the calibration curve in the steric/hyperlayer mode was calculated as −1.17 and −1.12 for the uniform and thickness-tapered channels, respectively. Linear regression for the steric calibration was conducted using the retention time data of PS standards (1−20 μm), showing linearity with particle sizes. Linear plots in the normal mode of separation (left linear plots) were obtained by the linear regression of retention time data of PS standards (0.02−0.3 μm) against diameter because the theoretical retention time in a thickness-tapered channel was not yet clearly expected. Therefore, the steric inversion diameter was empirically determined from the crossing point of the two calibration curves. As shown in the plot, the empirical steric inversion diameter values (0.69 and 0.62 μm) calculated for the two channels were not significantly different from each other. The similar diameters indicate that the increase in inlet thickness of the thickness-tapered channel compared to that of the uniform channel with similar void volumes does not significantly alter the steric inversion diameter.

CONCLUSIONS

This study demonstrated that a thickness-tapered channel in an FlFFF can be utilized as an alternative to increase the separation speed without applying a programmed variation in migration flow rate. In particular, the thickness-tapered channel offered certain advantages in steric/hyperlayer separation compared to the normal mode operation because it induced an increase in hydrodynamic lift forces, which can be useful for eluting long-retaining particles without incorporating field programming or reducing channel thickness. Reduction of channel thickness is beneficial for high-speed separation in the steric/hyperlayer mode; however, this approach can deteriorate the resolution in separating large-diameter particles. Increasing the migration flow rate to accelerate the elution of long-retaining small-diameter particles induces a dilution effect during typical UV detection. Thus, the use of a channel with a relatively thicker inlet and a thinner outlet can be an alternative approach to ensure good differentiation of particle equilibrium at the beginning of migration and maintain the resolving power for particles of an upper large-diameter limit and a faster separation of particles of a smaller size limit than that of a uniform channel with a similar void volume, consequently expanding the dynamic size range of separation to a certain extent. Moreover, the slight improvement in elution recovery could be an additional feature of the thickness-tapered channel. The present study demonstrated the possibility of employing a channel with tapering thickness for the first time. Further studies are needed to examine the performance of a thickness-tapered channel with different tapering thickness gradients in comparison to the field-programmed separation of a uniform channel and to elucidate the retention theory in a channel of varying thicknesses.

AUTHOR INFORMATION

Corresponding Author

Myeong Hee Moon − *Department of Chemistry, Yonsei University, Seoul 03722, South Korea;* orcid.org/0000-0002-5454-2601; Phone: (82) 2 2123 5634; Email: mhmoon@yonsei.ac.kr; Fax: (82) 2 364 7050

Authors

Seung Yeon Shin − *Department of Chemistry, Yonsei University, Seoul 03722, South Korea;* orcid.org/0000-0001-6973-6647

Jae Won Seo − *Department of Chemistry, Yonsei University, Seoul 03722, South Korea*

Jin Yong Kim − *Department of Chemistry, Yonsei University, Seoul 03722, South Korea*

Philip Stephen Williams − *Cambrian Technologies Inc, Cleveland, Ohio 44109, United States;* orcid.org/0000-0002-5951-2612

Complete contact information is available at: https://pubs.acs.org/10.1021/acs.analchem.2c03503

Author Contributions

The manuscript was written through the contributions of all authors. All the authors approved the final version of the manuscript.

Notes

The authors declare no competing financial interest.

ACKNOWLEDGMENTS

This study was supported by a grant from the National Research Foundation (NRF) of Korea (NRF-2021R1A2C2003171).

https://doi.org/10.1021/acs.analchem.2c03503
Anal. Chem. 2022, 94, 14460−14466

REFERENCES

(1) Giddings, J. C. *Anal. Chem.* **1981**, *53*, 1170−1178.
(2) Giddings, J. C. *Science* **1993**, *260*, 1456−1465.
(3) Moon, M. H. *TrAC, Trends Anal. Chem.* **2019**, *118*, 19−28.
(4) Wahlund, K. G.; Winegarner, H. S.; Caldwell, K. D.; Giddings, J. C. *Anal. Chem.* **1986**, *58*, 573−578.
(5) Ratanathanawongs, S. K.; Lee, I.; Giddings, J. C. *ACS Symp. Ser.* **1991**, *472*, 229−246.
(6) Reschiglian, P.; Zattoni, A.; Roda, B.; Casolari, S.; Moon, M. H.; Lee, J.; Jung, J.; Rodmalm, K.; Cenacchi, G. *Anal. Chem.* **2002**, *74*, 4895−4904.
(7) Yang, J. S.; Lee, J. Y.; Moon, M. H. *Anal. Chem.* **2015**, *87*, 6342−6348.
(8) Kim, J. Y.; Lim, H. B.; Moon, M. H. *Anal. Chem.* **2016**, *88*, 10198−10205.
(9) Williams, P. S.; Lee, S. H.; Giddings, J. C. *Chem. Eng. Commun.* **1994**, *130*, 143−166.
(10) Ratanathanawongs, S. K.; Giddings, J. C. *Chromatographia* **1994**, *38*, 545−554.
(11) Williams, P. S.; Koch, T.; Giddings, J. C. *Chem. Eng. Commun.* **1992**, *111*, 121−147.
(12) Goldman, A. J.; Cox, R. G.; Brenner, H. *Chem. Eng. Sci.* **1967**, *22*, 653−660.
(13) Williams, P. S.; Moon, M. H.; Giddings, J. C.Fast separation and characterization of micron size particles by sedimentation/steric field-flow fractionation: Role of lift forces. In*Particle Size Analysis*; Stanley-Wood, N. G., Lines, R. W., Eds.; Royal Society of Chemistry: Cambridge, 1992; pp 280−289.
(14) Martin, M.; Beckett, R. *J. Phys. Chem. A* **2012**, *116*, 6540−6551.
(15) Jensen, K. D.; Williams, S. K.; Giddings, J. C. *J. Chromatogr. A* **1996**, *746*, 137−145.
(16) Dou, H.; Lee, Y. J.; Jung, E. C.; Lee, B. C.; Lee, S. *J. Chromatogr. A* **2013**, *1304*, 211−219.
(17) Moon, M. H.; Lee, K. H.; Min, B. R. *J. Microcolumn Sep.* **1999**, *11*, 676−681.
(18) Kim, Y. B.; Yang, J. S.; Moon, M. H. *J. Chromatogr. A* **2018**, *1576*, 131−136.
(19) Moon, M. H.; Williams, P. S.; Kang, D. J.; Hwang, I. *J. Chromatogr. A* **2002**, *955*, 263−272.
(20) Ratanathanawongs, S. K.; Giddings, J. C. *Anal. Chem.* **1992**, *64*, 6−15.
(21) Williams, P. S. *J. Microcolumn Sep.* **1997**, *9*, 459−467.
(22) Ahn, J. Y.; Kim, K. H.; Lee, J. Y.; Williams, P. S.; Moon, M. H. *J. Chromatogr. A* **2010**, *1217*, 3876−3880.
(23) Giddings, J. C.; Yang, F. J.; Myers, M. N. *Science* **1976**, *193*, 1244−1245.

https://doi.org/10.1021/acs.analchem.2c03503
Anal. Chem. 2022, 94, 14460−14466